Thermoelectric Power Factor Limit of a 1D Nanowire

I-Ju Chen,* Adam Burke, Artis Svilans, Heiner Linke, and Claes Thelander†
Solid State Physics and NanoLund, Lund University, Box 118, 22100 Lund, Sweden

(Received 29 September 2017; revised manuscript received 6 March 2018; published 24 April 2018)

In the past decade, there has been significant interest in the potentially advantageous thermoelectric properties of one-dimensional (1D) nanowires, but it has been challenging to find high thermoelectric power factors based on 1D effects in practice. Here we point out that there is an upper limit to the thermoelectric power factor of nonballistic 1D nanowires, as a consequence of the recently established quantum bound of thermoelectric power output. We experimentally test this limit in quasiballistic InAs nanowires by extracting the maximum power factor of the first 1D subband through *I-V* characterization, finding that the measured maximum power factors conform to the theoretical limit. The established limit allows the prediction of the achievable power factor of a specific nanowire material system with 1D electronic transport based on the nanowire dimension and mean free path. The power factor of state-of-the-art semiconductor nanowires with small cross section and high crystal quality can be expected to be highly competitive (on the order of $\mathrm{mW/m\,K^2}$) at low temperatures. However, they have no clear advantage over bulk materials at, or above, room temperature.

DOI: 10.1103/PhysRevLett.120.177703

Thermoelectric devices can convert heat gradients into electricity or pump heat by using electricity and thus have applications both in energy harvesting and solid-state refrigeration. A long-standing challenge for the widespread use of thermoelectric applications is to find material systems with increased energy conversion efficiency as well as higher power output. For a temperature difference $\Delta T \ll T$, the maximum power output density ($\mathrm{J\,m^{-3}}$) is proportional to the power factor of the material $S^2\sigma$, with Seebeck coefficient S and electrical conductivity σ. The pioneering theoretical work of Hicks and Dresselhaus [1] identified that a high $S^2\sigma$ can be achieved by one-dimensional (1D) charge channels in extremely thin quantum wires with high mobility. A similar analysis, also based on the Boltzmann transport equation, approximated the electron scattering time τ by a power law of energy E, $\tau(E) \sim E^r$, and indicated that $S^2\sigma$ could increase, in principle, indefinitely with increasing mobility, scattering parameter r, and decreasing nanowire (NW) cross section area. [2] In this picture, a NW can potentially have an unlimited power production ability as r diverges. The expected large $S^2\sigma$, together with the low thermal conductivity in NWs, led to the prediction of high energy conversion efficiency, triggering widespread efforts to develop NW-based thermoelectric materials.

Experimentally, however, the predicted high $S^2\sigma$ based on 1D electronic transport in NWs has to date not been observed. Thermoelectric properties of ballistic quasi-1D systems, including conductance quantization at multiples of $2e^2/h$ and oscillating Seebeck coefficient as a function of gate voltage, were first studied in quantum point contacts (QPCs) [3,4], but the values of power production or power factors were not explicitly extracted. In NWs, 1D effects are often obscured due to scattering and formation of quantum-dot-like states [5]. Nevertheless, conductance plateaus and Seebeck coefficient oscillations have been observed [6,7]. However, accurate extraction of reliable values for the power factor in 1D NWs has not been possible: first, because, as pointed out in Refs. [6,7], it is difficult to measure the Seebeck voltage at high NW impedance, the condition under which the peak power factor is expected; second, because the transport properties of single-NW devices are susceptible to device lengths and defect distributions. Therefore, it is critical to measure the conductance and Seebeck voltage simultaneously on the same NW segment, which is challenging [7].

Recently, Whitney established that the power production by a 1D channel is intrinsically limited by quantum effects [8,9]. This prediction, which is based on nonlinear scattering theory, indicates that a 1D electronic channel only has a limited ability to produce power through the thermoelectric effect—described by its power factor S^2G, with conductance of the system G. It is worth noting that the term *power factor* is used for both $S^2\sigma$ and S^2G, which are related to the thermoelectric power density and power, respectively. S^2G is often preferred for mesoscopic systems where a local description of electrical conduction is not adequate [10]. Nonetheless, the quantum limit is only attainable when the transport is ballistic. Therefore, the question arises: What is the maximum S^2G that can be measured directly in nonballistic 1D electronic channels, and as a result, what is the achievable $S^2\sigma$ in realistic NWs?

 © 2018 American Physical Society

Here we address this question by establishing a theoretical upper bound for the power factor (both $S^2\sigma$ and S^2G) of a nonballistic 1D NW and by testing this limit through measurements of the power factor of single-InAs nanowire devices. First, based on the theory of the quantum bound of thermoelectric power output and considering nonunitary electron transmission, we formulate a theoretical limit of S^2G in nonballistic 1D channels. Then, in the experiment, we study conductance quantization and Seebeck coefficient oscillations, which are the characteristics of 1D subband transport. We use current voltage (I-V) characterization to directly and simultaneously measure the electrical conductance and Seebeck voltage on the same InAs nanowire segments. We demonstrate that the theoretical limit is consistent with the measured S^2G maximum. Finally, by considering that the transmission probability of electrons scale classically with device lengths, we establish the limit of $S^2\sigma$ in nonballistic 1D NWs to provide an indicator for the optimal $S^2\sigma$ that can be achieved with 1D charge transport in realistic NW structures.

For ballistic 1D channels, Whitney derived that the maximum power output is equal to the quantum bound $P_{\rm QB} = B_0(\pi^2/h)k_B^2\Delta T^2$ with $B_0 \approx 0.0321$ [8,9]. Thus, the power factor quantum bound for a spin-degenerate 1D channel is [11]

$$(S^2G)_{\rm QB} = 2\times 4B_0\frac{\pi^2}{h}k_B^2 \approx 0.73\ ({\rm pW/K^2}), \qquad (1)$$

based on the relation $P_{\rm max} = (S^2G)\times\Delta T^2/4$ [12], where $P_{\rm max}$ is a thermoelectric system's maximum power output and the factor of 2 is due to spin degeneracy. In quasiballistic and diffusive 1D channels, the transmission probability of charge carriers is less than unity, and we can extend the derivation of $(S^2G)_{\rm QB}$ to provide a power factor upper bound for these transport regimes as well. The transmission probability can be expressed as $T(E) = T_{\rm max}\phi(E)$, where $T_{\rm max}$ describes the maximum height of $T(E)$, and $\phi(E)$ is a normalized function that describes the shape of $T(E)$. In Refs. [8,9], it is shown that a step function is the optimal transmission function shape to maximize the thermoelectric power output. Therefore, a 1D channel with $T(E) = T_{\rm max}\phi(E)$ has a S^2G upper bound that can be calculated by considering $T(E) = T_{\rm max}\theta(E)$, where $\theta(E)$ is a Heaviside step function.

G and S of the spin-degenerate 1D channel can then be described by the Landauer formalisms as [11,13]

$$G = \frac{2e^2}{h}\int T(E)\frac{-\partial f}{\partial E}dE = \frac{2e^2}{h}T_{\rm max}\int \phi(E)\frac{-\partial f}{\partial E}dE \qquad (2)$$

and

$$S = G^{-1}\frac{2e}{hT(K)}\int T(E)(E-E_F)\frac{\partial f}{\partial E}dE = G^{-1}\frac{2e}{hT(K)}T_{\rm max}\int \phi(E)(E-E_F)\frac{\partial f}{\partial E}dE, \qquad (3)$$

where $f(E)$ is the Fermi-Dirac distribution, with Fermi level E_F, and $T(K)$ is the temperature. With $T(E) = T_{\rm max}\theta(E)$, G becomes the ballistic 1D conductance scaled by $T_{\rm max}$, and S becomes the ballistic 1D Seebeck coefficient independent of $T_{\rm max}$. Thus, we obtain the theoretical S^2G limit of nonballistic 1D channels

$$(S^2G)_{\rm limit} = T_{\rm max}\times(S^2G)_{\rm QB}. \qquad (4)$$

How close the actual S^2G is to $(S^2G)_{\rm limit}$ depends on $\phi(E)$, which is determined by the exact scattering mechanisms.

In order to test this limit, we simultaneously measure G and Seebeck voltage $V_{th} = S\Delta T$ of individual InAs NW back-gate field-effect transistors. Figure 1(a) shows such a transistor with the InAs NW (60 ± 4 nm diameter) lying on a SiO_2 (150 nm)/Si substrate. The material growth [14] and device fabrication details are described in the Supplemental Material [15]. We perform electrical and thermoelectric characterization with the circuitry shown in Fig. 1(b) in a variable temperature probe station. In the thermoelectric measurements, the side Joule heater creates a thermal bias ΔT between the contacts. Under the thermal bias, the electrical current I through the device can be expressed as $I(V) = G(V + V_{th})$ in the linear regime. We measure $I(V)$ and deduce G and V_{th} using linear fits [23]. With this method, we can reliably extract S^2G for up to 1 MΩ device impedance. ΔT is calibrated with resistance thermometry using the source and drain four-probe metal lines (Supplemental Material [15]). In some cases, ΔT is measured in the absence of the NW or on a different device with nominally identical structure. Modeling of the device temperature using a finite element method (Supplemental Material [15]) finds negligible variations in the measured ΔT, as the temperature profile along the substrate surface is dominated by the thermal conduction of the substrate [24]. It also confirms that the thermometer temperature is a good representation of the average temperature at the metal-NW contact.

As shown in Fig. 2(a), we observe conductance quantization in the V_g-dependent conductance measurement at $T = 10$ K with $V = 1$ mV. The observations are consistent with the electrical conduction through a spin-degenerate

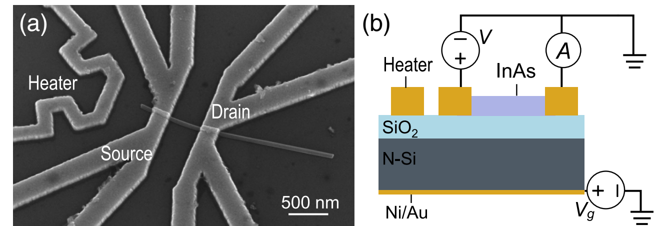

FIG. 1. (a) Scanning electron micrograph of an InAs NW back-gate field-effect transistor with a side Joule heater. Figures 3(a) and (d) shows the experimental data of this exact device. (b) Schematic of the device and circuitry, where a source-drain bias V and a back-gate voltage V_g are applied to the device.

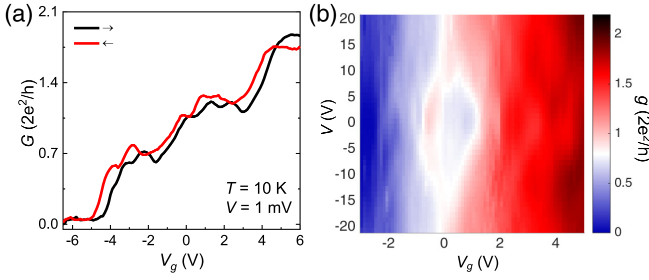

FIG. 2. (a) $G\ (V_g)$ measured with increasing (→) and decreasing (←) V_g, and with $V = 1$ mV for a device with $L = 180$ nm. (b) Differential conductance $g = dI/dV$ measured as a function of V_g and V for a device with $L = 275$ nm.

quasi-1D system [25–27]. In the ballistic limit, the conductance is an integer of $2e^2/h$, whereas in the quasiballistic and diffusive regime, a lowering of the conductance steps is due to reduced electron transmission probabilities. The conductance step associated with the nth subband can be approximated to $T_{n,\max}(2e^2/h)$, where $T_{n,\max}$ is the maximum height of $T(E)$ of the nth subband. In short devices, when sweeping V and V_g, the differential conductance $g = dI/dV$ exhibits a diamond-shaped area with g roughly equal to the quantized conductance values [Fig. 2(b)], which is a feature of ballistic quasi-1D transport [25,26]. Outside the diamond, g deviates from the quantized values, as the number of occupied subbands is different at the two terminals [25,26]. The top and bottom tips of the diamond-shaped region correspond to when $E_{F,S}$ and $E_{F,D}$ align with two different subband edges, from which an approximately 15–20 meV spacing between the first and second subband can be extracted. This value agrees with the calculated energy difference, 18 meV, between the first and the degenerate second and third electronic states in a 60 nm diameter hexagonal confinement with $0.026\,m_e$ effective mass [28] (Supplemental Material [15]). In Fig. 2(a), the similar height of each conductance step indicates that the degeneracy of the second or third quantum state and thus the rotational symmetry are broken, possibly due to the asymmetric electrostatic potential induced by the source, drain, and gate contacts.

Next, we measure G and $V_{th} = S\Delta T$ [Figs. 3(a) and 3(b)] simultaneously through $I(V)$ measurement to extract S^2G [Fig. 3(c)]. In connection to the conductance quantization, S shows oscillations that are characteristic of 1D subband transport. S can be described by substituting $T(E)$ with the total transmission through multiple subbands $\sum_n T_n(E)$ in the Landauer formalism [Eqs. (2) and (3)]. The magnitude and sign of S depend on the balance between electron transport above and below E_F. Inferring from Eq. (2), the onset of each G step comes from the population of a new 1D subband, i.e., when E_F is close to a subband edge [Fig. 3(a), inset (1)]. Under this condition, S is nonzero because within an energy range $\sim k_BT$ there are more transport channels for $E > E_F$. Conversely, the G plateau occurs when E_F is more than $\sim k_BT$ away from any subband edges [Fig. 3(a), inset (2)]. In this case, S will approach zero because within $\sim k_BT$ there is approximately as much transport from states above

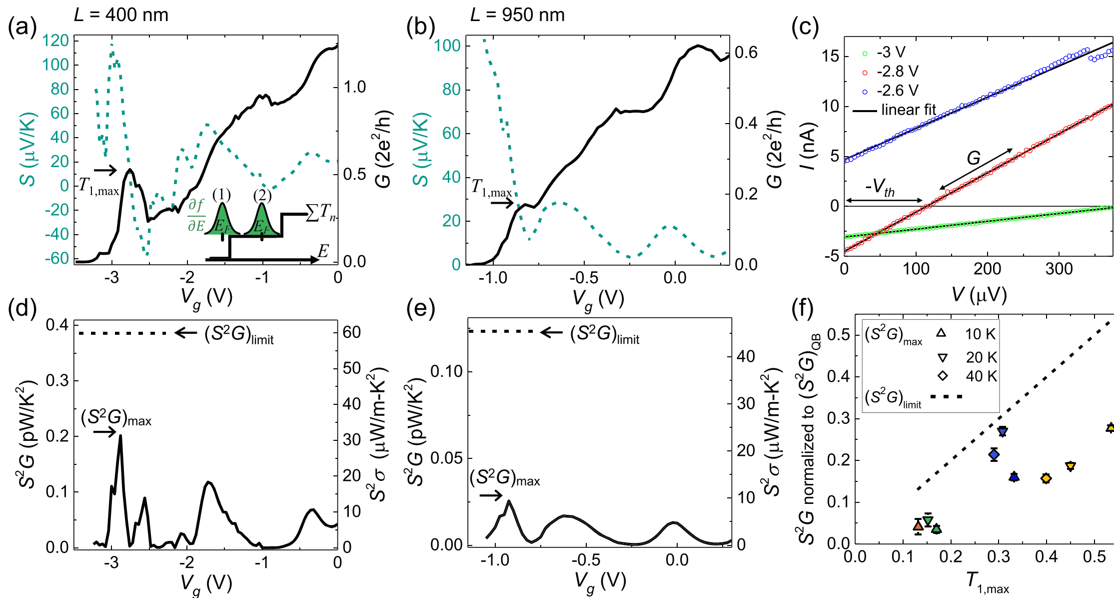

FIG. 3. (a),(b) $G\ (V_g)$ and $S\ (V_g)$ measured in $L = 400$ and 950 nm devices. $T_{1,\max}$ can be estimated from the first conductance step height. (Inset) Schematics of $\sum_n T_n(E)$ through a quasi-1D system, where $T_n\,(E)$ is assumed to be a constant. The df/dE distribution is plotted for (1) E_F within $\sim k_BT$ from the band edge and (2) E_F more than $\sim k_BT$ away from the band edges. (c) Linear fitting is used to extract $V_{th} = S\Delta T$ and G from the same I-V curves. (d),(e) V_g-dependent S^2G and $S^2\sigma$ and the theoretical limit $(S^2G)_{\rm limit}$ (dashed lines). (f) $(S^2G)_{\max}$ for devices with $L = 950$ (green), 820 (orange), 310 (blue), and 400 nm (yellow) at $T = 10$, 20, and 40 K and $(S^2G)_{\rm limit}$ as a function of $T_{1,\max}$.

and below E_F. One exception being that when E_F is decreased below the first subband edge, given that the valence band is far away, S will increase continuously as there are no states below E_F. Overall, S and the deduced S^2G show a decaying oscillation as a function of V_g [Figs. 3(d) and 3(e)]. These features compare qualitatively well with theoretical and experimental studies of QPCs [3,4], confirming the interpretation that the thermoelectric properties are dominated by quasi-1D transport. Yet the observed electronic transport is nonballistic, and the scattering processes have a visible influence on the measured G and S. For example, we observe a dip in G before the onset of each G step and the concurrent sign change in S [Fig. 3(a)], which resembles the theoretically predicted channel opening effect [29].

We note that, in order to consider systems with different ballisticity, a generalized Landauer formalism [30,31] is used here, where the transmission $T(E)$ is an effective value that includes both elastic and inelastic scattering.

As expected, the maximum S^2G, $(S^2G)_{\max}$, is found near the depletion of the first subband [Figs. 3(d) and 3(e)]. At temperatures 10–40 K, k_BT is much smaller than the first and second subband spacing; therefore, we attribute the measured $(S^2G)_{\max}$ solely to electron transport through the first subband. The first conductance step heights [indicated by arrows in Figs. 3(a) and 3(b)] provide an estimation of the maximum electron transmission probability $T_{1,\max}$ through the first subband, at least within the relevant energy range. Based on this maximum, $(S^2G)_{\text{limit}}$ can be calculated using Eq. (4). We find in Figs. 3(d)–3(f) that $(S^2G)_{\max}$ and $(S^2G)_{\text{limit}}$ are within the same order of magnitude and $(S^2G)_{\max}$ shows an increasing trend with $T_{1,\max}$, in agreement with $(S^2G)_{\text{limit}}$.

We now further discuss the implication of the S^2G upper bound on the value of $S^2\sigma$. If we consider that the resistance due to different scattering processes in the transport channel adds classically, it follows that, in the quasiballistic and diffusive transport regime, the transmission probability of charge carriers is [13,27,32]

$$T_n = \frac{\lambda_n}{L_c + \lambda_n}, \tag{5}$$

where λ_n is the electron mean free path and L_c is the channel length. Considering that L_c only deviates slightly from the device length L, by combining Eqs. (4) and (5), $(S^2G)_{\text{limit}}$ can be modified to obtain the theoretical upper bound for $S^2\sigma$,

$$(S^2\sigma)_{\text{limit}} = (S^2G)_{\text{limit}} \times \frac{L}{A} < (S^2G)_{\text{QB}} \times \frac{\lambda_{1,\max}}{A}, \tag{6}$$

where $\lambda_{1,\max}$ is the maximum electron mean free path of the first subband. This expression directly connects the limit of $S^2\sigma$ in a 1D NW to the quantum limit of thermoelectric power production. $(S^2\sigma)_{\text{limit}}$, as opposed to $(S^2G)_{\text{limit}}$, can be used to compare with materials across different dimensions.

From the observed conductance step heights [Figs. 2(a), 3(a), 3(b), and 4(a)], we find $T_{1,\max} = 0.9$–0.07 for devices with $L = 180$–1240 nm. We set $L_c = L - 2\delta$, where δ is a fitting parameter that accounts for the downward band bending near the source and drain contact [Fig. 4(b)] caused by the metal-semiconductor work function difference, sulfur passivation penetration, and/or possible imperfections in semiconductor-metal contacts. By fitting the experimental values with Eq. (5), we obtain $\overline{\lambda_{1,\max}} = 232 \pm 81$ nm and $\bar{\delta} = 79 \pm 101$ nm. Based on Eq. (6), we can extract $(S^2\sigma)_{\text{limit}} \approx 72\ \mu\text{W/m K}^2$ for the ensemble of NWs measured in this study, which is consistent with the measured values $(S^2\sigma)_{\max} = 12$–$43\ \mu\text{W/m K}^2$ at temperatures between 10 and 40 K.

$(S^2\sigma)_{\text{limit}}$ is a clear upper limit, unlike $S^2\sigma$ predicted by semiclassical calculations, which can increase unlimitedly with temperature or by changing the energy dependence of the relaxation time [2]. Equation (6) provides an explicit guide to understanding what values of $S^2\sigma$ can be achieved with existing NWs and highlights that small NW cross section combined with long electron mean free path are needed to achieve large $S^2\sigma$. For example, InAs NWs with 28×40 nm cross section area and 930 nm electron mean free path at 4 K were recently demonstrated [33]. According to Eq. (6), such NWs can be expected to have a $S^2\sigma$ of around 0.8 mW/m K^2 with single-subband transport at 4 K. In comparison, for bulk InAs, scaling the theoretical estimates of $S^2\sigma$ to similar mean free paths provides $S^2\sigma < 60\ \mu\text{W/m K}^2$ at 4 K [5]. This large advantage of 1D NWs at low temperatures is possible because $(S^2\sigma)_{\text{limit}}$ of a 1D electronic channel [Eq. (6)] depends on temperature only indirectly through the mean free path, which is generally longer at low temperatures and

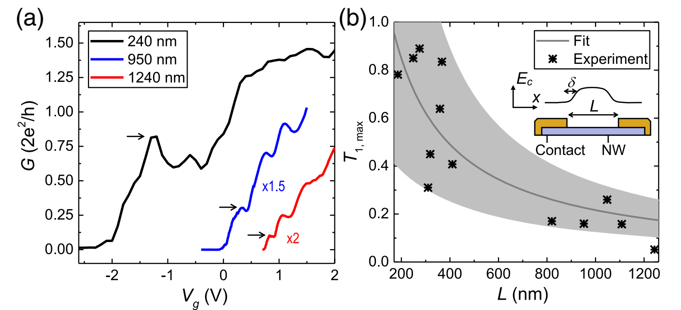

FIG. 4. (a) $G(V_g)$ for devices with $L = 240$, 950, and 1240 nm. For devices with $L = 950$ and 1240 nm, G is scaled by 1.5 and 2.5 times, respectively. The arrows indicate the first conductance step heights, which are used to extract $T_{1,\max}$. (b) Extracted $T_{1,\max}$ from devices with various L (black asterisks), fitted with Eq. (5) (gray line). The gray area indicates the standard deviation of the fit. (Inset) An illustration of the fitting parameter δ used to account for the downward band bending near the metal contacts.

thus gives larger $(S^2\sigma)_{\text{limit}}$, while theoretical calculations based on the Boltzmann transport equation showed that $S^2\sigma$ of bulk materials is drastically reduced at low temperatures [2,5]. Thus, one does not expect the same advantage at room temperature or higher, where the experimental value of $S^2\sigma$ of bulk InAs is around 2 mW/m K^2 at 300 K [34], and even higher $S^2\sigma$ has been achieved in bulk materials with large charge effective mass [35,36].

We emphasize that the theoretical limits in Eqs. (4) and (6) only consider one electronic subband. This assumption suffices when k_BT is much smaller than the first and second 1D subband spacing. However, when k_BT is comparable to or larger than the subband spacing, then higher subbands need to be included in the calculations. Such calculations showed that NWs with intermediate diameters have a lower $S^2\sigma$ relative to the 1D and bulk limits [37,38].

In conclusion, we experimentally extract the power factor of single-nanowire devices that have 1D electronic transport. The extracted power factors are comparable to, but below, the quantum bound, which we attribute to nonballistic transport. First, we showed that the quantum bound of thermoelectric power production leads to a stringent limit on the power factor S^2G of a nonballistic 1D electronic system. Experimental observation of conductance quantization and Seebeck coefficient oscillation then allowed us to identify 1D electronic transport and extract the maximum S^2G of the first subband, which conformed to the proposed limit. However, for practical applications, the thermoelectric power density is often of interest. Therefore, we also established the limit on the power factor $S^2\sigma$ of an effective medium made of closely packed nanowires stretching into the diffusive transport regime. This limit provides an explicit guide on the optimal $S^2\sigma$ that can be achieved in realistic nanowire structures. These findings are helpful for quantitative predictions and to better inform and guide future efforts to improve the thermoelectric performance of 1D nanowires.

The authors thank Luna Namazi for providing the nanowires and Martin Leijnse for helpful discussion and acknowledge financial support from the People Programme (Marie Curie Actions) of the European Union's Seventh Framework Programme (FP7-People-2013-ITN) under REA Grant agreement No. 608153, PhD4Energy, the Swedish Research Council Grant No. 2015-00619, and Marie Sklodowska Curie Actions, Cofund, Project INCA 600398, the Swedish Energy Agency (Project No. P38331-1), the Knut and Alice Wallenberg Foundation (Project No. 2016.0089), and NanoLund.

*i-ju.chen@ftf.lth.se
†claes.thelander@ftf.lth.se

[1] L. D. Hicks and M. S. Dresselhaus, Thermoelectric figure of merit of a one-dimensional conductor, Phys. Rev. B **47**, 16631 (1993).
[2] N. T. Hung, E. H. Hasdeo, A. R. T. Nugraha, M. S. Dresselhaus, and R. Saito, Quantum Effects in the Thermoelectric Power Factor of Low-Dimensional Semiconductors, Phys. Rev. Lett. **117**, 036602 (2016).
[3] H. van Houten, L. W. Molenkamp, C. W. J. Beenakker, and C. T. Foxon, Thermo-electric properties of quantum point contacts, Semicond. Sci. Technol. **7**, B215 (1992).
[4] L. W. Molenkamp, Th. Gravier, H. van Houten, O. J. A. Buijk, M. A. A. Mabesoone, and C. T. Foxon, Peltier coefficient and thermal conductance of a quantum point contact, Phys. Rev. Lett. **68**, 3765 (1992).
[5] P. M. Wu, J. Gooth, X. Zianni, S. Fahlvik Svensson, J. G. Gluschke, K. A. Dick, C. Thelander, K. Nielsch, and H. Linke, Large thermoelectric power factor enhancement observed in InAs nanowires, Nano Lett. **13**, 4080 (2013).
[6] Y. Tian, M. R. Sakr, J. M. Kinder, D. Liang, M. J. MacDonald, R. L. J. Qiu, H.-J. Gao, and X. P. A. Gao, One-dimensional quantum confinement effect modulated thermoelectric properties in InAs nanowires, Nano Lett. **12**, 6492 (2012).
[7] P. Mensch, S. Karg, V. Schmidt, B. Gotsmann, H. Schmid, and H. Riel, One-dimensional behavior and high thermoelectric power factor in thin indium arsenide nanowires, Appl. Phys. Lett. **106**, 093101 (2015).
[8] R. S. Whitney, Most Efficient Quantum Thermoelectric at Finite Power Output, Phys. Rev. Lett. **112**, 130601 (2014).
[9] R. S. Whitney, Finding the quantum thermoelectric with maximal efficiency and minimal entropy production at given power output , Phys. Rev. B **91**, 115425 (2015).
[10] H. Bruus and K. Flensberg, *Many-Body Quantum Theory in Condensed Matter Physics: An Introduction* (Oxford University Press, New York, 2004).
[11] R. Kim, S. Datta, and M. S. Lundstrom, Influence of dimensionality on thermoelectric device performance, J. Appl. Phys. **105**, 034506 (2009).
[12] G. Benenti, G. Casati, K. Saito, and R. S. Whitney, Fundamental aspects of steady-state conversion of heat to work at the nanoscale, Phys. Rep. **694**, 1 (2017).
[13] S. Datta, *Quantum Transport: Atom to Transistor* (Cambridge University Press, Cambridge, England, 2005).
[14] M. Nilsson, L. Namazi, S. Lehmann, M. Leijnse, K. A. Dick, and C. Thelander, Single-electron transport in InAs nanowire quantum dots formed by crystal phase engineering, Phys. Rev. B **93**, 195422 (2016).
[15] See Supplemental Material http://link.aps.org/supplemental/10.1103/PhysRevLett.120.177703 for a detailed description of the nanowire growth and device fabrication, the temperature measurement and simulation, and the calculation of the quantum confinement energy, which includes Refs. [14,16–22,28].
[16] L. L. Isaacs, Low-temperature specific heat of gold, silver, and copper, J. Chem. Phys. **43**, 307 (1965).
[17] G. K. White, The thermal conductivity of gold at low temperatures, Proc. Phys. Soc. London Sect. A **66**, 559 (1953).
[18] J. Ederth, L. B. Kish, E. Olsson, and C. G. Granqvist, Temperature dependent electrical resistivity in nanocrystalline gold films made by advanced gas deposition, J. Appl. Phys. **88**, 6578 (2000).
[19] R. C. Zeller and R. O. Pohl, Thermal conductivity and specific heat of noncrystalline solids, Phys. Rev. B **4**, 2029 (1971).

[20] W. J. de Haas and T. Biermasz, The thermal conductivity of KBr, KC1 and SiO_2 at low temperatures, Physica **4**, 752 (1937).

[21] P. H. Kezsom and G. Seidel, Specific heat of germanium and silicon at low temperatures, Phys. Rev. **113**, 33 (1959).

[22] M. E. Brinson and W. Dunstant, Thermal conductivity and thermoelectric power of heavily doped *n*-type silicon, J. Phys. C **3**, 483 (1970).

[23] S. Roddaro, D. Ercolani, M. A. Safeen, S. Suomalainen, F. Rossella, F. Giazotto, L. Sorba, and F. Beltram, Giant thermovoltage in single InAs nanowire field-effect transistors, Nano Lett. **13**, 3638 (2013).

[24] M.-H. Bae, Z. Li, Z. Aksamija, P. N. Martin, F. Xiong, Z.-Y. Ong, I. Knezevic, and E. Pop, Ballistic to diffusive crossover of heat flow in graphene ribbons, Nat. Commun. **4**, 1734 (2013).

[25] L. P. Kouwenhoven, B. J. van Wees, C. J. P. M. Harmans, J. G. Williamson, H. van Houten, C. W. J. Beenakker, C. T. Foxon, and J. J. Harris, Nonlinear conductance of quantum point contacts, Phys. Rev. B **39**, 8040 (1989).

[26] J. Kammhuber, M. C. Cassidy, H. Zhang, O. Gul, F. Pei, M. W. A. de Moor, B. Nijholt, K. Watanabe, T. Taniguchi, D. Car *et al.*, Conductance quantization at zero magnetic field in InSb nanowires, Nano Lett. **16**, 3482 (2016).

[27] S. Chuang, Q. Gao, R. Kapadia, A. C. Ford, J. Guo, and A. Javey, Ballistic InAs nanowire transistors, Nano Lett. **13**, 555 (2013).

[28] A. Belabbes, C. Panse, J. Furthmuller, and F. Bechstedt, Electronic bands of III-V semiconductor polytypes and their alignment, Phys. Rev. B **86**, 075208 (2012).

[29] I. Kander, Y. Imry, and U. Sivan, Effects of channel opening and disorder on the conductance of narrow wires, Phys. Rev. B **41**, 12941 (1990).

[30] J. L. D'Amato and H. M. Pastawski, Conductance of a disordered linear chain including inelastic scattering events, Phys. Rev. B **41**, 7411 (1990).

[31] H. M. Pastawski, Classical and quantum transport from generalized Landauer-Bttiker equations, Phys. Rev. B **44**, 6329 (1991).

[32] T. Markussen, R. Rurali, A.-P. Jauho, and M. Brandbyge, Scaling Theory Put into Practice: First-Principles Modeling of Transport in Doped Silicon Nanowires, Phys. Rev. Lett. **99**, 076803 (2007).

[33] J. Gooth, M. Borg, H. Schmid, V. Schaller, S. Wirths, K. Moselund, M. Luisier, S. Karg, and H. Riel, Ballistic one-dimensional InAs nanowire cross-junction interconnects, Nano Lett. **17**, 2596 (2017).

[34] N. Mingo, Thermoelectric figure of merit and maximum power factor in III-V semiconductor nanowires, Appl. Phys. Lett. **84**, 2652 (2004).

[35] L.-D. Zhao, G. Tan, S. Hao, J. He, Y. Pei, H. Chi, H. Wang, S. Gong, H. Xu, V. P. Dravid, C. Uher, G. J. Snyder, C. Wolverton, and M. G. Kanatzidis, Ultrahigh power factor and thermoelectric performance in hole-doped single-crystal SnSe, Science **351**, 141 (2016).

[36] G. Tan, L.-D. Zhao, and M. G. Kanatzidis, Rationally designing high-performance bulk thermoelectric materials, Chem. Rev. **116**, 12123 (2016).

[37] J. E. Cornett and O. Rabin, Thermoelectric figure of merit calculations for semiconducting nanowires, Appl. Phys. Lett. **98**, 182104 (2011).

[38] J. E. Cornett and O. Rabin, Universal scaling relations for the thermoelectric power factor of semiconducting nanostructure, Phys. Rev. B **84**, 205410 (2011).